Structure of a complex between a voltage-gated calcium channel β-subunit and an α-subunit domain

Filip Van Petegem, Kimberly A. Clark, Franck C. Chatelain & Daniel L. Minor Jr

Cardiovascular Research Institute, Departments of Biochemistry and Biophysics, and Cellular and Molecular Pharmacology, University of California San Francisco, 513 Parnassus Avenue, Box 0130, San Francisco, California 94143, USA

Voltage-gated calcium channels (Ca_Vs) govern muscle contraction, hormone and neurotransmitter release, neuronal migration, activation of calcium-dependent signalling cascades, and synaptic input integration[1]. An essential Ca_V intracellular protein, the β-subunit ($Ca_V\beta$)[1,2], binds a conserved domain (the α-interaction domain, AID) between transmembrane domains I and II of the pore-forming α_1 subunit[3] and profoundly affects multiple channel properties such as voltage-dependent activation[2], inactivation rates[2], G-protein modulation[4], drug sensitivity[5] and cell surface expression[6,7]. Here, we report the high-resolution crystal structures of the $Ca_V\beta_{2a}$ conserved core, alone and in complex with the AID. Previous work suggested that a conserved region, the β-interaction domain (BID), formed the AID-binding site[3,8]; however, this region is largely buried in the $Ca_V\beta$ core and is unavailable for protein–protein interactions. The structure of the AID–$Ca_V\beta_{2a}$ complex shows instead that $Ca_V\beta_{2a}$ engages the AID through an extensive, conserved hydrophobic cleft (named the α-binding pocket, ABP). The ABP–AID interaction positions one end of the $Ca_V\beta$ near the intracellular end of a pore-lining segment, called IS6, that has a critical role in Ca_V inactivation[9,10]. Together, these data suggest that $Ca_V\beta$s influence Ca_V gating by direct modulation of IS6 movement within the channel pore.

The 1.97 Å resolution structure of the $Ca_V\beta_{2a}$ core shows that $Ca_V\beta$s comprise two well-conserved domains (Fig. 1a). The first, an SH3 fold, contains five antiparallel β-strands (β1–β5), a 3_{10} helix (η1), and two α-helices (α1 and α2) that lie amino-terminal to β1 and carboxy-terminal to β4, respectively. The strand that completes the SH3 fold, β5 (residues 217–224), is separated in the primary structure from the core of the SH3 domain by approximately 70 residues (variable domain 2, V2, a site of splice variation and amino acid insertions and deletions[2]) that are absent from the structure (Fig. 1b). The second conserved domain consists of a five-stranded parallel β-sheet (β6–β10), surrounded by six α-helices (α3–α8) and two 3_{10} helices (η2 and η3), and is related to the core of nucleotide kinase enzymes.

$Ca_V\beta$s share structural features with membrane-associated guanylate kinases (MAGUKs), a protein scaffold family that organizes signalling components near membranes[11]. MAGUKs contain one or more PDZ domains N-terminal to an SH3 domain, a bridging region known as a HOOK domain and a nucleotide kinase domain[11,12]. PDZ domains are approximately 100 residues long. The $Ca_V\beta_{2a}$ structure indicates that $Ca_V\beta$s lack N-terminal PDZ domains. There are too few residues N-terminal to the SH3 domain (even in $Ca_V\beta_{1b}$, the $Ca_V\beta$ with the longest (55 amino acids) N-terminal variable region 1, V1) to fold as a PDZ domain. The absence of a PDZ domain distinguishes $Ca_V\beta$s from canonical MAGUK proteins.

Comparison of $Ca_V\beta_{2a}$ with a representative MAGUK, PSD-95 (refs 12, 13), reveals other differences. Superposition of the nucleotide kinase domains shows that the relative orientations of the SH3 and nucleotide kinase domains differ by approximately 90°, an arrangement that makes $Ca_V\beta_{2a}$ a more elongated structure (Fig. 2a). The nucleotide kinase domain of MAGUKs is homologous to guanylate kinases and retains guanosine monophosphate (GMP) binding, but key residues for enzymatic function are missing[12]. The four-stranded β-sheet nucleotide kinase subdomain that binds GMP in MAGUKs is absent in $Ca_V\beta_{2a}$ (Fig. 2a). Furthermore, two $Ca_V\beta_{2a}$ loops (between β7–η2 and β8–β9) occlude part of the binding site for the GMP guanosine ring. Thus, the $Ca_V\beta$ nucleotide kinase domain seems to have lost the ability to bind nucleotides.

The structures of $Ca_V\beta_{2a}$ and PSD-95 SH3 domains are similar (Fig. 2b). Neither is compatible with canonical modes of proline-rich ligand binding. Both lack the aromatic residues necessary for ligand engagement[13], and the surface that would bind polyproline ligands is blocked by the α2 helix[12,13]. In PSD-95, residues C-terminal to the nucleotide kinase domain contribute an extra SH3 β-strand that is absent from canonical SH3 domains[13] and absent in $Ca_V\beta_{2a}$. The HOOK domain, present in MAGUKs and $Ca_V\beta_{2a}$, bridges SH3

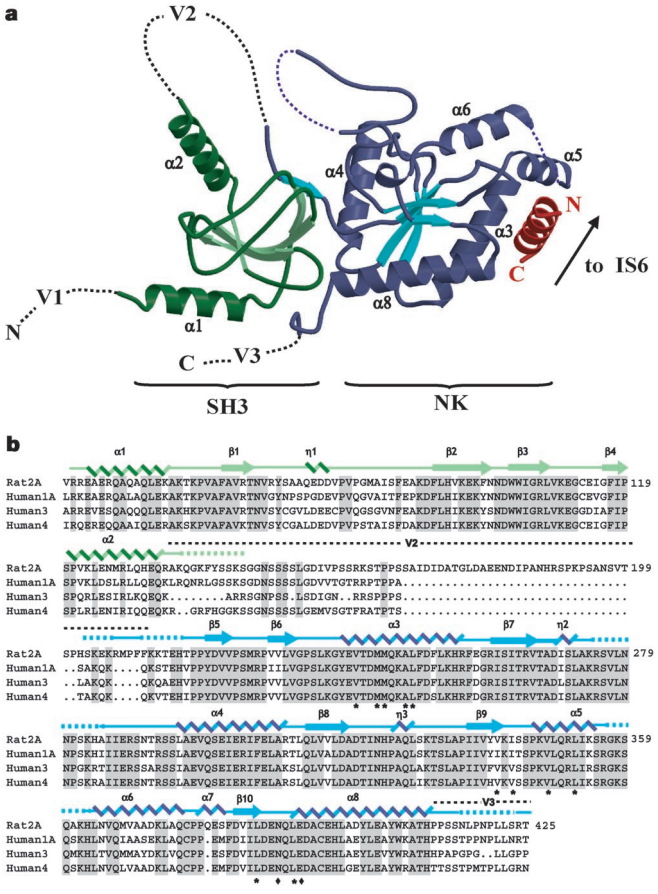

Figure 1 Structure of the $Ca_V\beta_{2a}$–$Ca_V1.2$ AID complex. **a**, Ribbon diagram of the complex. Dashed lines indicate regions absent from the structures. SH3 and nucleotide kinase (NK) domains are shown in green and blue, respectively. The AID is shown in red. $Ca_V\beta_{2a}$ α-helices are labelled. Variable regions V1, V2 and V3 are indicated. The $Ca_V\beta_{2a}$ unbound structure is similar to that shown here for the complex. The arrow indicates where the AID connects to transmembrane segment IS6. **b**, Sequence alignment of representatives of each $Ca_V\beta$ isoform. The top sequence shows residues 40–425 of rat $Ca_V\beta_{2a}$. Numbers on the right denote each line's terminal residue. Shading denotes residues identical among isoforms. The two $Ca_V\beta_{2a}$ domains used for crystallization are indicated in green and blue, respectively. Secondary structure elements are indicated: α, α-helix; η, 3_{10} helix; β, β-strand. Dashed lines indicate residues present in the crystallized constructs but absent in the electron density. Location of the V2 and part of the V3 regions are shown. Asterisks identify residues that contribute side-chain contacts to the AID-binding pocket; diamonds mark side chains with direct hydrogen bonds to the AID.

β-strands β4 and β5 and comprises α2 and variable domain 2 of $Ca_V\beta_{2a}$. HOOK domains are important regulatory regions for interactions of MAGUKs with other proteins[11,12,14] and may serve a similar function for $Ca_v\beta$ protein–protein interactions.

$Ca_v\beta$s exert their effects on Ca_V function by binding the pore-forming α_1 subunit at a conserved, 18-residue sequence located between membrane domains I and II (the AID)[3,15] (Fig. 3a). Interpretation of mutagenesis and biochemical studies suggested that $Ca_v\beta$–AID interactions occur through a 41-residue segment ($Ca_V\beta_{2a}$ residues 212–252) termed the β-interaction domain (BID)[8,16]. The $Ca_V\beta_{2a}$ structure shows that the central region of the BID, which includes the residues previously thought to be important for BID–AID interactions[8], is entirely buried and cannot participate directly in protein–protein interactions (Fig. 3b). Two putative BID phosphorylation sites[8,16] are also buried in this region. Given the extent of burial, mutations used to determine the relative importance of residues involved in BID–AID interactions (for example, proline to arginine)[8] are likely to have abolished AID binding by disrupting the folded structure of the nucleotide kinase domain rather than by perturbing direct AID contacts. Although it would appear that the $Ca_V\beta_{2a}$ structure conflicts with previous data, most of the supporting evidence for the BID–AID interaction relied on indirect functional experiments and direct BID–AID binding was never demonstrated[8,16].

If the BID does not interact directly with the AID, how do $Ca_v\beta_{2a}$ and the AID interact? To answer this, we solved the high-resolution (2.00 Å) structure of a complex between the conserved $Ca_V\beta_{2a}$ core and an 18-residue peptide containing the AID from the L-type channel $Ca_v1.2$. The electron density reveals the first 16 residues of the AID and the location of the binding pocket on $Ca_v\beta_{2a}$ (Fig. 3c). Overall, the $Ca_v\beta_{2a}$ structure is very similar to the unbound form (root-mean-square deviation $(RMSD)_{C\alpha} = 0.397$ Å) and bears only a few conformational changes in side chains near the AID-binding pocket ($Ca_v\beta_{2a}$ residues M244, N390, E393 and R351). The AID forms an α-helix that is anchored to the binding pocket through a set of conserved residues (AID residues L434, G436, Y437, W440

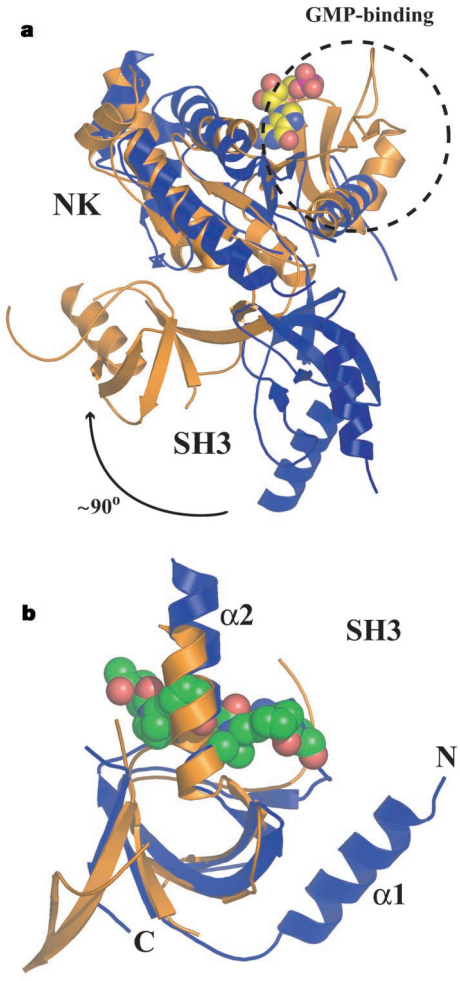

Figure 2 Structural comparisons between PSD-95 (gold) and $Ca_V\beta_{2a}$ (blue). **a**, Superposition of $Ca_V\beta_{2a}$ and PSD-95 nucleotide kinase domains ($RMSD_{C\alpha} = 3.9$ Å). The dashed circle indicates the guanosine-monophosphate (GMP)-binding domain present in PSD-95 but absent in $Ca_V\beta_{2a}$. The guanosine monophosphate molecule bound to PSD-95 is displayed in space-filling representation. Nucleotide kinase (NK) and SH3 domains are indicated. The relative change in SH3 domain orientation is indicated. **b**, Superposition of PSD-95 and $Ca_V\beta_{2a}$ SH3 domains ($RMSD_{C\alpha} = 1.6$ Å). Position of the polyproline ligand from a superposition with the Sem5 SH3 domain (Protein Data Bank code 2SEM) ($RMSD_{C\alpha} = 1.8$ Å) is shown in space-filling representation. The Sem5 SH3 is not shown. The DALI server generated the superpositions (http://www.ebi.ac.uk/dali/).

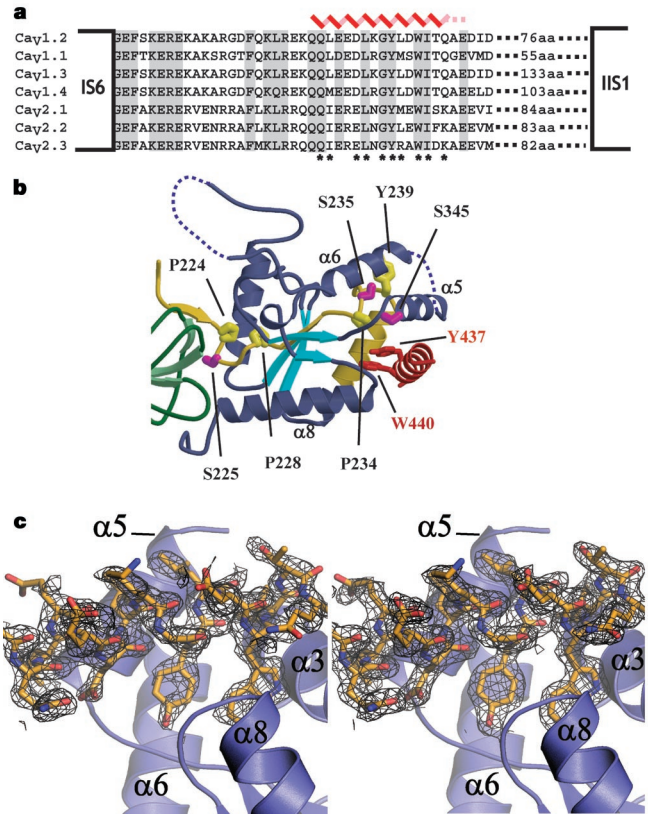

Figure 3 Features of the AID–$Ca_V\beta_{2a}$ interaction and location of the previously described BID. **a**, Sequence alignment of AID domains ($Ca_V1.2$ residues 428–445) and neighbouring residues. The positions of the last transmembrane segment of transmembrane domain I (IS6) and the first transmembrane segment of transmembrane domain II (IIS1) are shown. Secondary structure of the AID from the co-crystal structure is indicated (red). Dashed lines indicate residues absent from the electron density. Asterisks identify side-chain contacts with $Ca_V\beta_{2a}$ closer than 4 Å. **b**, Position of the previously described BID (residues 212–252; yellow)[3,8]. Residues previously proposed to mediate AID–BID interactions (P224, P228, P234, Y239) are indicated and have relative accessibilities of 1.4%, 0%, 0% and 32.4%. Putative PKC sites S225, S235 and S345 are also shown (magenta) and have relative accessibilities of 8.8%, 0% and 35.4%, respectively. S345 accessibility reduces to 12% in the complex. Accessibility values are relative to a tripeptide, Gly-X-Gly. **c**, The left panel shows $F_o - F_c$ electron density, contoured at 2σ, for the AID–$Ca_V\beta_{2a}$ complex before building the AID. The right panel shows final $2F_o - F_c$ density, contoured at 1σ, for the AID from the refined AID–$Ca_V\beta_{2a}$ structure (right). In both panels the final AID model is shown.

NATURE | doi:10.1038/nature02588 | www.nature.com/nature

and I441) that are important for $Ca_V\beta$ binding and for α-subunit modulation by $Ca_V\beta$s[8,15,17]. These residues bind a deep groove that we call the α-binding pocket (ABP), formed by helices α3, α5 and α8 of the $Ca_v\beta_{2a}$ nucleotide kinase domain at a site distal to the SH3 domain (Figs 1a, 3b and 4a).

The complex buries approximately 730 $Å^2$ of ABP surface, of which about 350 $Å^2$ are hydrophobic. AID side chains D433, W440 and Q443 make direct hydrogen bonds to the ABP (Supplementary Fig. 1). The depth and extent of burial of the aromatic AID positions Y437 and W440 is particularly striking (Fig. 4b, c). The AID Y437 hydroxyl group is central to a buried hydrogen bond network comprising three water molecules, AID residue D433 and five $Ca_V\beta_{2a}$ residues (Supplementary Fig. 1). Mutation of this tyrosine to phenylalanine greatly diminishes AID–$Ca_V\beta$ binding[15]. The extensive AID–ABP interactions are consistent with biochemical experiments demonstrating strong AID–$Ca_V\beta$ interaction (dissociation constant ~6–20 nM)[18]. The $Ca_V\beta$ side chains that contact the AID are highly conserved among $Ca_V\beta$ isoforms (see Figs 1b, 3a and 4a; see also Supplementary Fig. 1). Thus, both binding partners engage each other through conserved residues to create the AID–ABP interaction.

Interactions between the $Ca_V\alpha_1$ and $Ca_V\beta$ subunits markedly influence the cell surface expression of functional channels[6,7]. Control of Ca_V trafficking by regulating $Ca_V\alpha_1$–$Ca_V\beta$ interactions is emerging as an important means of modulating cellular excitability[7]. Ca_V channel subtypes are major clinical targets for drugs that treat cardiovascular disease, migraine and pain[19]. Development of compounds that could interfere with the AID–ABP binding interactions might provide new ways to modulate Ca_V function in pathological states.

The $Ca_V\beta$–AID structure provides a starting point for understanding how $Ca_V\beta$ modulates numerous channel properties. G-protein βγ subunits (Gβγ) inhibit Ca_V function[1,4]; however, the sites of Gβγ–Ca_V interactions and precise inhibitory mechanisms remain highly controversial[4]. Biochemical experiments show that Gβγ binds the Ca_V2 AID and that mutations at AID positions Q1, Q2, R5, L7, G9 and Y10 (corresponding to $Ca_v1.2$ AID residues 428, 429, 432, 434, 436 and 437) abolish Gβγ–AID binding[20]. In contrast, other studies suggest that the *in vitro* Gβγ–AID interaction is functionally irrelevant and that the relevant Gβγ-binding determinants lie elsewhere in the channel cytoplasmic domains[21,22]. The structure of the $Ca_V\beta_{2a}$–AID complex shows that three of the putative Gβγ–AID interacting positions (L7, G9 and Y10), which are invariant in Ca_V1 and Ca_V2 channels (Fig. 3a), are deeply buried by interactions with $Ca_V\beta$ (Fig. 4a, b; see also Supplementary Fig. 2 and Table 2). The extent of burial of these residues, which are critical for maintaining $Ca_V\beta$–AID association[3,15], suggests that Gβγ and $Ca_V\beta$ cannot bind to the AID simultaneously. Taken together with the observation that the Gβγ–AID affinity is at least 10–20-fold weaker than the $Ca_V\beta$–AID[20] affinity, the structure also indicates that it is unlikely that Gβγ could effectively compete with $Ca_V\beta$ for AID binding without drastic structural rearrangement of the $Ca_V\beta$–AID complex. Thus, our data lend support to the view that the major Gβγ interaction sites lie in other Ca_V cytoplasmic domains[21–23].

How might $Ca_V\beta$s affect channel gating? Although the detailed

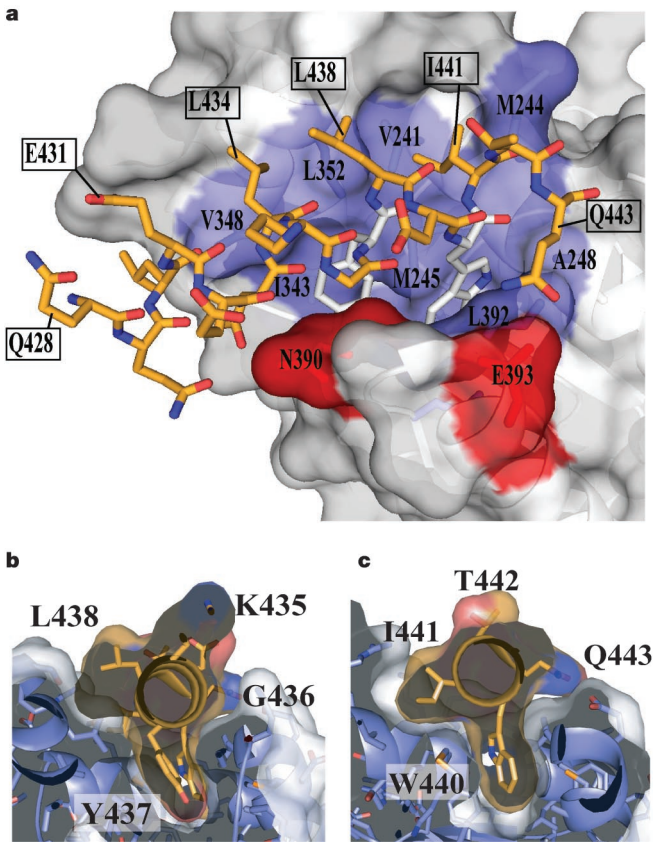

Figure 4 AID–ABP interactions. **a**, Surface representation of the $Ca_V\beta_{2a}$ ABP, bound to the AID. The AID (gold) is shown in stick representation. Y437 and W440 are white. $Ca_V\beta_{2a}$ residues that contribute hydrophobic (blue) and hydrogen bond (red) side-chain contacts to the AID are labelled. Select residues of the AID are labelled to orient the reader. **b**, **c**, Slices through the AID–ABP interaction at AID positions Y437 and W440 (gold). Labels indicate the AID residues.

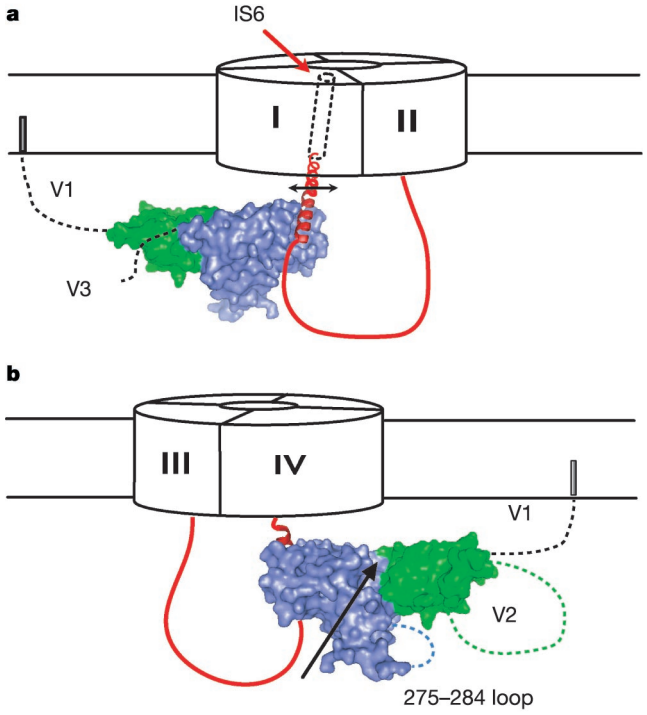

Figure 5 Cartoon of proposed model for how $Ca_V\beta$ affects $Ca_V\alpha_1$ gating. **a**, Orientation of $Ca_V\beta_{2a}$ with respect to the I–II loop (red), pore-forming subunit, and connection to IS6. In $Ca_V\beta_{2a}$, variable region 1 (V1) is tethered to the membrane. The I–II loop between the AID N terminus and IS6 is depicted as a helix. $Ca_V\beta_{2a}$ SH3 and nucleotide kinase domains are coloured green and blue, respectively. The arrow indicates that $Ca_V\beta$ couples to IS6 movements (rotations, translations or both). **b**, View from the opposite side of **a**. The groove between SH3 and nucleotide kinase domains (demarcated by the arrow) and two flexible $Ca_V\beta_{2a}$ regions, the 275–284 loop and variable region 2 (V2), are on the same $Ca_V\beta$ face, opposite the ABP. These regions may interact with other pore-forming subunit cytoplasmic domains.

mechanisms of Ca_V inactivation processes remain unknown, functional experiments show that the IS6 pore-lining segment has a key role[10]. Motions of pore-lining transmembrane segments are a common theme emerging in ion channel gating[24,25]. Twenty-two residues separate the AID helix N terminus from the cytoplasmic end of IS6. We do not know the structure, but sequence evaluation suggests that these residues have a high helix propensity and could readily form a continuous helix between the AID helix and the presumed transmembrane helix of IS6 (Fig. 5a). AID residue 5 (E432, here) slows inactivation when negatively charged (as in Ca_V1 channels) and speeds inactivation when positively charged (as in Ca_V2 channels)[26,27]. This residue is exposed on the surface of the AID helix (Fig. 4a) where it would be available to interact with other parts of the channel and could influence the rates of movement of the $Ca_V\beta$–AID complex and therefore IS6. The profound inactivation rate slowing caused by $Ca_V\beta_{2a}$ requires anchoring of the N terminus to the membrane by palmitoylation[28]. Orientation of the AID helix towards IS6 places the N-terminal membrane anchor on the periphery of the α_1 subunit and suggests that $Ca_V\beta_{2a}$ slows channel inactivation by restricting the movement of the IS6 transmembrane domain. $Ca_V\beta$s have a deep groove between the SH3 and nucleotide kinase domains that is on the same face as the V2 domain. These features may be used to engage other cytoplasmic parts of the channel[29,30] and allow $Ca_V\beta$ to couple motions in other channel domains directly to IS6 through AID attachment.

The structures presented here represent the first high-resolution view of any part of the voltage-gated calcium channel, and provide an important step towards understanding the detailed molecular mechanism models for how Ca_Vs function. This work strongly suggests that $Ca_V\beta$ affects Ca_V gating properties by directly influencing conformational changes that are likely to occur in the channel pore[10]. □

Methods

The crystal structures of recombinant $Ca_V\beta_{2a}$ and $Ca_V\beta_{2a}$–AID complexes were solved to resolutions of 1.97 Å and 2.00 Å, respectively. The final R/R_{free} values are 18.55%/21.32% for $Ca_V\beta_{2a}$ and 19.97%/24.15% for the $Ca_V\beta_{2a}$–AID complex. Figures were prepared with PyMOL, MOLSCRIPT and RASTER3D. The experimental details for protein expression, purification, crystallization, structure solution, statistics of data collection, phasing and refinement are available as Supplementary Information.

Received 1 March; accepted 23 April 2004; doi:10.1038/nature02588.
Published online 12 May 2004.

1. Catterall, W. A. Structure and regulation of voltage-gated Ca^{2+} channels. *Annu. Rev. Cell Dev. Biol.* **16,** 521–555 (2000).
2. Dolphin, A. C. β-subunits of voltage-gated calcium channels. *J. Bioenerg. Biomembr.* **35,** 599–620 (2003).
3. Pragnell, M. *et al.* Calcium channel β-subunit binds to a conserved motif in the I–II cytoplasmic linker of the α1-subunit. *Nature* **368,** 67–70 (1994).
4. Dolphin, A. C. G protein modulation of voltage-gated calcium channels. *Pharmacol. Rev.* **55,** 607–627 (2003).
5. Hering, S. β-Subunits: fine tuning of Ca^{2+} channel block. *Trends Pharmacol. Sci.* **23,** 509–513 (2002).
6. Bichet, D. *et al.* The I–II loop of the Ca^{2+} channel α1 subunit contains an endoplasmic reticulum retention signal antagonized by the β subunit. *Neuron* **25,** 177–190 (2000).
7. Beguin, P. *et al.* Regulation of Ca^{2+} channel expression at the cell surface by the small G-protein kir/Gem. *Nature* **411,** 701–706 (2001).
8. De Waard, M., Scott, V. E., Pragnell, M. & Campbell, K. P. Identification of critical amino acids involved in α1-β interaction in voltage-dependent Ca^{2+} channels. *FEBS Lett.* **380,** 272–276 (1996).
9. Stotz, S. C., Hamid, J., Spaetgens, R. L., Jarvis, S. E. & Zamponi, G. W. Fast inactivation of voltage-dependent calcium channels. A hinged-lid mechanism? *J. Biol. Chem.* **275,** 24575–24582 (2000).
10. Zhang, J. F., Ellinor, P. T., Aldrich, R. W. & Tsien, R. W. Molecular determinants of voltage-dependent inactivation in calcium channels. *Nature* **372,** 97–100 (1994).
11. Dimitratos, S. D., Woods, D. F., Stathakis, D. G. & Bryant, P. J. Signaling pathways are focused at specialized regions of the plasma membrane by scaffolding proteins of the MAGUK family. *Bioessays* **21,** 912–921 (1999).
12. Tavares, G. A., Panepucci, E. H. & Brunger, A. T. Structural characterization of the intramolecular interaction between the SH3 and guanylate kinase domains of PSD-95. *Mol. Cell* **8,** 1313–1325 (2001).
13. McGee, A. W. *et al.* Structure of the SH3-guanylate kinase module from PSD-95 suggests a mechanism for regulated assembly of MAGUK scaffolding proteins. *Mol. Cell* **8,** 1291–1301 (2001).
14. Paarmann, I., Spangenberg, O., Lavie, A. & Konrad, M. Formation of complexes between Ca^{2+}.calmodulin and the synapse-associated protein SAP97 requires the SH3 domain-guanylate kinase domain-connecting HOOK region. *J. Biol. Chem.* **277,** 40832–40838 (2002).
15. Witcher, D. R., De Waard, M., Liu, H., Pragnell, M. & Campbell, K. P. Association of native Ca^{2+} channel β subunits with the α1 subunit interaction domain. *J. Biol. Chem.* **270,** 18088–18093 (1995).
16. De Waard, M., Pragnell, M. & Campbell, K. P. Ca^{2+} channel regulation by a conserved β subunit domain. *Neuron* **13,** 495–503 (1994).
17. Berrou, L., Klein, H., Bernatchez, G. & Parent, L. A specific tryptophan in the I–II linker is a key determinant of β-subunit binding and modulation in Ca(V)2.3 calcium channels. *Biophys. J.* **83,** 1429–1442 (2002).
18. Opatowsky, Y., Chomsky-Hecht, O., Kang, M. G., Campbell, K. P. & Hirsch, J. A. The voltage-dependent calcium channel β subunit contains two stable interacting domains. *J. Biol. Chem.* **278,** 52323–52332 (2003).
19. Kochegarov, A. A. Pharmacological modulators of voltage-gated calcium channels and their therapeutical application. *Cell Calcium* **33,** 145–162 (2003).
20. De Waard, M. *et al.* Direct binding of G-protein βγ complex to voltage-dependent calcium channels. *Nature* **385,** 446–450 (1997).
21. Zhang, J. F., Ellinor, P. T., Aldrich, R. W. & Tsien, R. W. Multiple structural elements in voltage-dependent Ca^{2+} channels support their inhibition by G proteins. *Neuron* **17,** 991–1003 (1996).
22. Qin, N., Platano, D., Olcese, R., Stefani, E. & Birnbaumer, L. Direct interaction of Gβγ with a C-terminal Gβγ-binding domain of the Ca^{2+} channel α1 subunit is responsible for channel inhibition by G protein-coupled receptors. *Proc. Natl Acad. Sci. USA* **94,** 8866–8871 (1997).
23. Ivanina, T., Blumenstein, Y., Shistik, E., Barzilai, R. & Dascal, N. Modulation of L-type Ca^{2+} channels by Gβγ and calmodulin via interactions with N and C termini of α1C. *J. Biol. Chem.* **275,** 39846–39854 (2000).
24. Miyazawa, A., Fujiyoshi, Y. & Unwin, N. Structure and gating mechanism of the acetylcholine receptor pore. *Nature* **424,** 949–955 (2003).
25. Jiang, Y. *et al.* The open pore conformation of potassium channels. *Nature* **417,** 523–526 (2002).
26. Herlitze, S., Hockerman, G. H., Scheuer, T. & Catterall, W. A. Molecular determinants of inactivation and G protein modulation in the intracellular loop connecting domains I and II of the calcium channel α1A subunit. *Proc. Natl Acad. Sci. USA* **94,** 1512–1516 (1997).
27. Berrou, L., Bernatchez, G. & Parent, L. Molecular determinants of inactivation within the I–II linker of α1E (CaV2.3) calcium channels. *Biophys. J.* **80,** 215–228 (2001).
28. Restituito, S. *et al.* The β2a subunit is a molecular groom for the Ca^{2+} channel inactivation gate. *J. Neurosci.* **20,** 9046–9052 (2000).
29. Walker, D. *et al.* A new β subtype-specific interaction in α1A subunit controls P/Q-type Ca^{2+} channel activation. *J. Biol. Chem.* **274,** 12383–12390 (1999).
30. Walker, D., Bichet, D., Campbell, K. P. & De Waard, M. A β4 isoform-specific interaction site in the carboxyl-terminal region of the voltage-dependent Ca^{2+} channel α1A subunit. *J. Biol. Chem.* **273,** 2361–2367 (1998).

Supplementary Information accompanies the paper on **www.nature.com/nature**.

Acknowledgements We thank J. M. Berger, K. Brejc, D. Fass, D. Julius, E. A. Lumpkin and B. A. Schulman for comments on the manuscript; J. Holton at beamline 8.3.1 at the Advanced Light Source for help with data collection; R. W. Tsien and D. T. Yue for the calcium channel clones; and members of the Minor laboratory for support at all stages of this work. This work was supported by awards to D.L.M. from the McKnight Foundation for Neuroscience, the March of Dimes Basil O'Connor Scholar program, the Alfred P. Sloan Foundation, and the Rita Allen Foundation. D.L.M. is a McKnight Foundation Scholar, an Alfred P. Sloan Research Fellow and a Rita Allen Foundation Scholar.

Competing interests statement The authors declare that they have no competing financial interests.

Correspondence and requests for materials should be addressed to D.L.M. (minor@itsa.ucsf.edu).
Coordinates and structure factors have been deposited in the Protein Data Bank under accession codes 1T0H and 1T0J.

Supplemental Figure 1

Van Petegem *et al.*

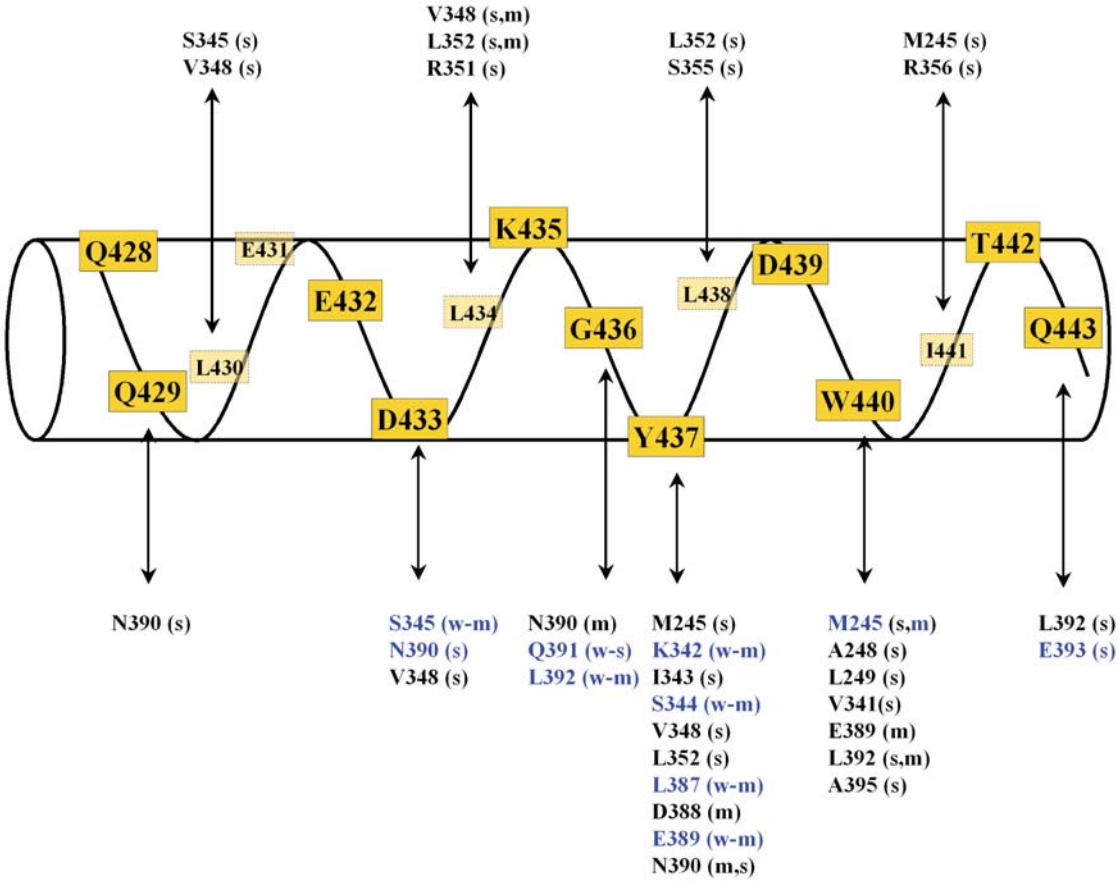

Supplemental Figure 1 Schematic representation of interactions between the AID peptide and $Ca_V\beta_{2a}$. All residues of $Ca_V\beta_{2a}$ with atoms closer than 4Å are indicated. 'm', indicates contacts with the main chain. 's', indicates contacts with the sidechain. Residues highlighted in blue form hydrogen bonds to the AID, either directly or via a water molecule ('w').

Supplemental Figure 2 **Van Petegem *et al.***

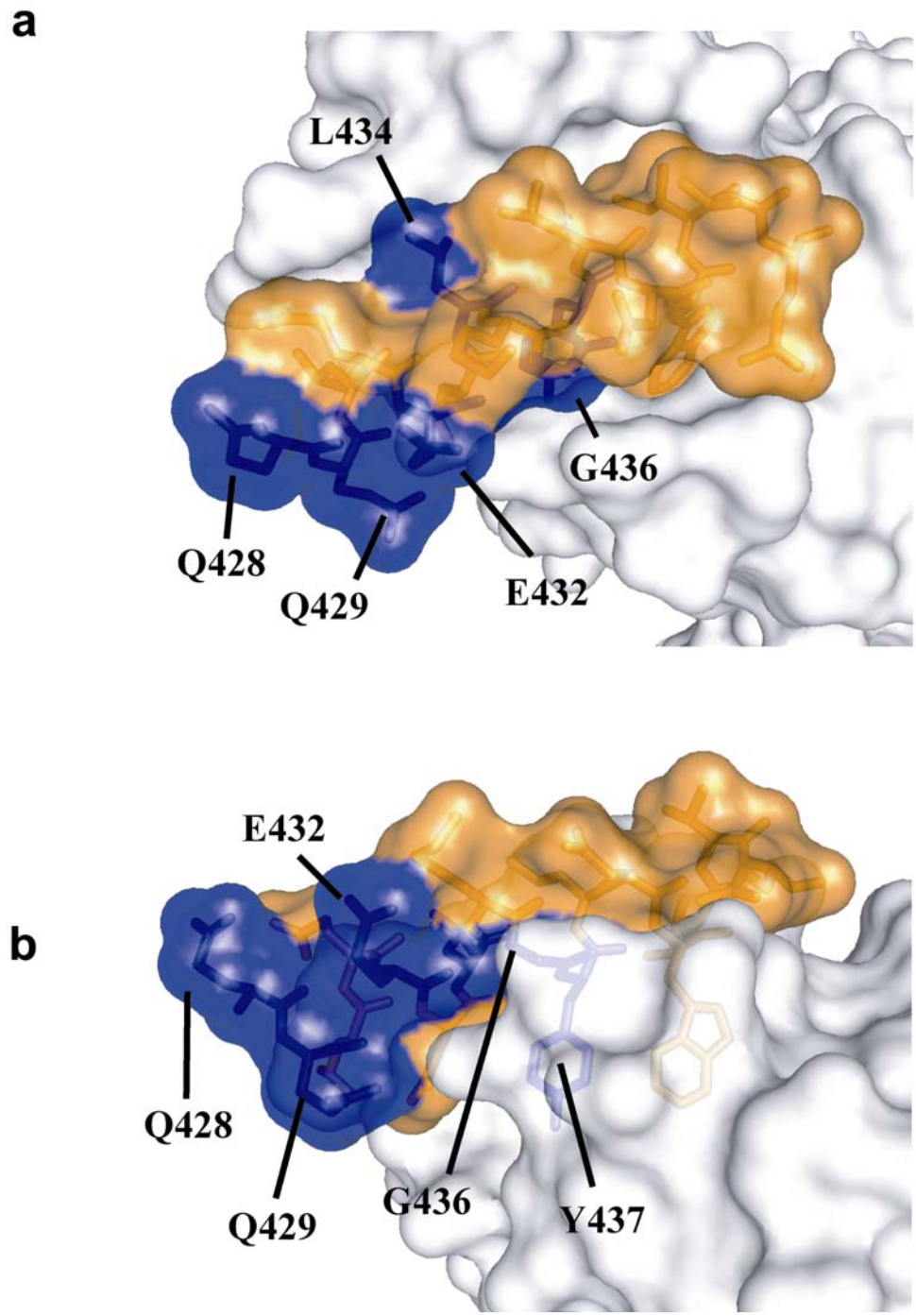

Supplemental Figure 2 a, b Location of AID residues implicated in Gβγ binding[1] (blue). Note that G_{436} and Y_{437} are buried in the complex.

Supplemental Table 1: Data collection, phasing and refinement.

	$Ca_V\beta_{2a}$		$Ca_V\beta_{2a}$-AID complex
	λ_1	λ_2	
Wavelength (Å)	1.0199	0.9796	1.1159
Resolution (Å)	30-1.97 (2.04-1.97)	30-2.20 (2.24-2.20)	30 – 2.00 (2.07-2.00)
Space group	P1		P1
Cell parameters (Å, °)	a=36.18, b=45.26, c=58.70 α=107.34, β=95.75, γ=97.00		a=36.76, b=45.33, c=60.65, α=96.813, β=102.459, γ=98.526
# unique reflections	24274 (2402)		24890 (2503)
R_{sym} * (%)	6.9 (30.5)	7.6 (29.2)	8.1 (38.5)
I/σ(I)	27.51 (2.45)	15.0 (4.2)	11.65 (2.06)
Completeness (%)	97.8 (96.5)	98.4 (97.5)	97.3 (96.1)
Mosaicity (°)	0.57		0.69
Phasing power **	0.36	1.24	n/a
Overall FOM□ (before/after density modification)	0.36 / 0.94		n/a
R_{cryst}/R_{free} (%)	18.55 / 21.32	n/a	19.97 / 24.15
# protein residues	283	n/a	299
# water molecules	147	n/a	138
Bond lengths RMSD (Å)	0.016	n/a	0.020
Bond Angles RMSD (°)	1.480	n/a	1.616
Mean overall B value ($Å^2$)	23.71	n/a	20.58
% Residues in core /disallowed regions of Ramachandran plot	93.5 / 0	n/a	93.1 / 0

- * $R_{sym} = \Sigma| I - \langle I \rangle | / \Sigma I$; I, intensity
- ** Phasing power = $[\Sigma_n|F_H|^2/\Sigma_n|E|^2]^{1/2}$; F_H, calculated heavy atom scattering factor; E, lack of closure error
- □ Figure of merit = $< |\Sigma_\alpha P(\alpha)e^{i\alpha}/\Sigma_\alpha P(\alpha)| >$; α, phase; $P(\alpha)$, phase probability distribution
- Values in parentheses refer to the highest resolution shell, where applicable

Supplemental Table 2: Accessibilities of AID residues in the AID-$Ca_V\beta_{2a}$ complex

Residue	Accessible surface area in AID-$Ca_V\beta_{2a}$ complex (Å^2)	Accessible surface area AID alone (Å^2)	% Accessible in AID-$Ca_V\beta_{2a}$ complex
Q 428	176	176	100.0
Q 429	125	135	92.5
L 430	49	123	39.8
E 431	88	109	80.7
E 432	101	112	90.1
D 433	**19**	**62**	**30.6**
L 434	**34**	**107**	**31.7**
K435	104	104	100.0
G 436	**1**	**39**	**2.5**
Y 437	**4**	**136**	**2.9**
L 438	62	97	63.9
D 439	77	92	83.7
W 440	**0**	**177**	**0.0**
I 441	**15**	**139**	**10.7**
T 442	124	124	100.0
Q 443	107	199	53.7

Comparison of the amount of accessible surface area of the AID. Values are shown for the conformation seen in the crystal structure in the presence and the absence of $Ca_V\beta_{2a}$. Residues that are in the complex (<35% accessible surface area are highlighted in bold.

Supplementary Methods:

Protein preparation Attempts to grow crystals of longer versions of rat $Ca_V\beta_{2a}$ failed due to solubility problems (full-length) or the formation of spherulites that could not be converted to crystals by extensive screening (constructs containing only the two conserved domains and V2). Therefore, we removed the V2 region and co-expressed the conserved domains as separate constructs corresponding to residues 17-145 (domain I) and 203-425 (domain II). Splitting the protein at the V2 loop has been shown to have minor effects on function[2]. Domain I was cloned into a modified pET28 vector (Novagen) containing in sequence, a His_6-tag, maltose binding protein (MBP), and a cleavage site for the Tobacco Etch Virus protease (TEV) (Gift of J.M. Berger). Domain II was cloned in pEGST [3] and expressed without affinity tags. The domains were co-expressed in *Escherichia coli* BL21(DE3) pLysS grown in 2xYT media at 37°C. Cells were lysed on ice by sonication in a buffer of 0.1M Tris-HCl, pH 8.0, containing 150 mM KCl, 10% sucrose, 1 mM EDTA, 5 mM β-mercaptoethanol, 1 mM PMSF. The complex was purified on a Poros20MC column (Perseptive Biosystems) in 250 mM KCl, 10 mM K-phosphate, pH 7.3, to retain His-tagged protein and eluted by a gradient to 300 mM imidazole in the same buffer. This step showed that domain II bound tightly to the His-tagged domain I. The protein was dialysed against 250 mM KCl, 10 mM K-phosphate, pH 7.3, and subjected to proteolytic cleavage with His-tagged TEV protease[4] at room temperature for ~12h. Uncleaved material, MBP, and protease were removed using a Poros20MC column and chromatographic conditions similar to those described above. Fractions that did not bind to the column were pooled and purified further with a Hiload SP column (Amersham) in 20mM MES, pH 6.3 and 1mM EDTA with a linear gradient from 250 mM to 600 mM KCl over eight column volumes. The resulting protein complex contained equal amounts of domains I & II and was dialysed against 20 mM KCl, 5 mM DTT, 10 mM Hepes, pH 7.0,

5 mM NaN_3 and concentrated to 5-15 mg ml^{-1} using Amicon Ultra concentrators (10K cutoff) (Millipore).

Selenomethionine-substituted domains I and II were co-expressed in BL21(DE3)pLysS cells in M9 minimal medium with 20% glucose as carbon source with the methionine biosynthesis pathway inhibited[5]. Purification was as described for native protein except that all buffers were supplemented with 5 mM methionine and 10 mM β-mercaptoethanol to prevent selenium oxidation.

The alpha interaction domain (AID) of human $Ca_v\alpha_1c$ (amino acid sequence QQLEEDLKGYLDWITQAE) was cloned into a modified pET27 vector (Novagen), pSV272, containing a His_6-tag, MBP, and a TEV cleavage site (gift of N. Pokala and T. Handel) and expressed in BL21(DE3)pLysS. Cells were lysed as described above. The purified complex of $Ca_V\beta_{2a}$ domains I+II was added to the lysate and the resulting complex with the AID was purified and concentrated using the protocol described for the I+II complex.

Crystallization and structure determination Complexes of native and selenomethionine-substituted $Ca_V\beta_{2a}$ domains I+II were crystallized by hanging-drop vapour diffusion[6] at 4°C by mixing 1μl of protein (5-15 mg ml^{-1}) with 1μl of well solution containing 0.1 M Tris-Cl , pH8.0, 0.2 M NaCl, & 10-20% PEG 4000. Crystals of the complex with AID were obtained in the same conditions by macroseeding with crystals of the $Ca_v\beta_{2a}$ domains I + II. X-ray diffraction data were collected at beamline 8.3.1 of the Advanced Light Source at Lawrence Berkeley National Laboratory. A two wavelength MAD-experiment was performed on crystals of SeMet-substituted domains I + II. The crystals belong to space group P1 and diffract to 1.97 Å. Location and refinement of seven selenium positions, phasing, and density modification were performed using CNS[7]. An

initial model was built using Arp/wArp[8] and manually completed using XtalView[9]. Two internal loops between η2 and α4, (residues 275-284) and α5 and α6 (residues 357-362) were not visible in the electron density. Two isolated stretches of residues at the N- and C-terminal ends of the NK domain (207-210 and 424-425) are ordered by crystal lattice contacts. One of these regions, the peptide RMPF (207-210), binds to a small groove on the surface of the SH3 domain of a neighbouring molecule in the lattice. We also measured a low-resolution dataset from a different crystal form (space group $P4_1$, data not shown), and solved this structure by molecular replacement. There were no significant changes in the main chains between the crystal forms. Crystals of the AID complex belong to the space group P1 and diffract to 2.00 Å. Due to significant differences in the unit cell dimensions, molecular replacement was performed with the uncomplexed structure using AMoRe[10]. All further refinement was performed using Refmac5[11], leading to final R/R_{free} factors of 18.55 % / 21.32% (uncomplexed) and 19.97 % and 24.15% (AID complex). Side chains and full residues with missing electron densities were not modelled.

References for Supplemental material:

1. De Waard, M. et al. Direct binding of G-protein betagamma complex to voltage-dependent calcium channels. *Nature* **385**, 446-50. (1997).

2. Opatowsky, Y., Chomsky-Hecht, O., Kang, M. G., Campbell, K. P. & Hirsch, J. A. The voltage-dependent calcium channel beta subunit contains two stable interacting domains. *J Biol Chem* **278**, 52323-32. Epub 2003 Oct 14. (2003).

3. Kholod, N. & Mustelin, T. Novel vectors for co-expression of two proteins in E. coli. *Biotechniques* **31**, 322-3, 326-8. (2001).

4. Kapust, R. B. et al. Tobacco etch virus protease: mechanism of autolysis and rational design of stable mutants with wild-type catalytic proficiency. *Protein Eng* **14**, 993-1000. (2001).

5. Van Duyne, G. D., Standaert, R. F., Karplus, P. A., Schreiber, S. L. & Clardy, J. Atomic structures of the human immunophilin FKBP-12 complexes with FK506 and rapamycin. *J Mol Biol* **229**, 105-24. (1993).

6. McPherson, A. *Crystallization of Biological Macromolecules* (Cold Spring Harbor Press, Cold Spring Harbor, NY, 1999).

7. Brunger, A. T. et al. Crystallography & NMR system: A new software suite for macromolecular structure determination. *Acta Crystallogr D Biol Crystallogr* **54**, 905-21. (1998).

8. Perrakis, A., Morris, R. & Lamzin, V. S. Automated protein model building combined with iterative structure refinement. *Nat Struct Biol* **6**, 458-63. (1999).

9. McRee, D. E. XtalView/Xfit--A versatile program for manipulating atomic coordinates and electron density. *J Struct Biol* **125**, 156-65. (1999).

10. Navaza, J. Implementation of molecular replacement in AMoRe. *Acta Crystallogr D Biol Crystallogr* **57**, 1367-72. (2001).

11. Collaborative Computational Project, N. The CCP4 suite: Programs for protein crystallography. *Acta Crystallogr D Biol Crystallogr* **50**, 760-763. (1994).